Reduced Heat Transport between Edge-Localized-Mode Bursts at Low Collisionality and Small Poloidal Larmor Radius

H. Urano, T. Takizuka, Y. Kamada, N. Oyama, H. Takenaga, and Y. Miura

Japan Atomic Energy Research Institute, Naka Fusion Research Establishment, Naka 319-0193, Japan

(Received 25 February 2005; published 13 July 2005)

Nondimensional parameter dependence of heat transport between edge localized modes (ELMs) is examined for H mode plasmas. The electron heat diffusivity between ELMs is reduced to the level of ion neoclassical transport in the plasma edge region which is affected by ELM burst. At lower edge collisionality, the heat flux assigned to the heat transport between ELMs is reduced and the ELM loss power is enhanced. During the inter-ELM phase, the energy confinement time becomes larger with decreasing the edge collisionality and poloidal Larmor radius.

DOI: 10.1103/PhysRevLett.95.035003 PACS numbers: 52.55.Fa, 52.25.Fi, 52.25.Xz

The H mode in tokamaks [1] is characterized by the structural formation of an edge transport barrier (ETB) at which heat transport is significantly reduced in contrast with a normal regime (L mode). The H mode is generally accompanied by the appearance of pulsating plasma heat losses called edge localized modes (ELMs) [2]. ELM bursts originate from edge magnetohydrodynamic (MHD) instabilities driven by a large edge pressure gradient and/or a bootstrap current that cause periodic expulsion of plasma energy.

Among various kinds of ELMs, the repetitive occurrence of isolated giant bursts called type-I ELMs [2,3] has been widely observed in the H mode accompanied with high energy confinement. Because of a possibility of serious impact on the plasma facing components, this kind of ELM has been intensively studied. The condition for the occurrence of type-I ELM bursts was observed to be close to the ideal MHD stability boundary against a coupled peeling-ballooning mode at intermediate toroidal mode number [4]. The existence of ELMs enables the H mode phase to be operated in a quasi-steady state in a global time scale with a moderate particle confinement avoiding the accumulation of impurities. Therefore, the H mode state accompanied by ELMs (or the ''ELMy H mode'') is associated with cyclical self-regulating dynamics that consist of two phases: (i) an ELM burst generated by the MHD destabilization rapidly enhancing instantaneous heat and particle losses at the plasma edge; (ii) a quiescent phase recovering the plasma energy and particle content.

For the interest of predicting the peak heat load onto plasma facing components in a fusion reactor, experimental characterization of energy pulses expelled by ELM bursts has been developed recently due to highly improved temporal resolution of magnetic measurements [5–8]. However, little is known about heat transport that occurs during the phase between ELMs (or the ''inter-ELM phase''). Understanding the process responsible for heat transport during the inter-ELM phase is of the utmost importance for a completed system of the self-regulating dynamics of ELMy H mode plasmas. The modeling of ELMy H mode involving MHD instabilities and anomalous transport process strongly requires the experimental evidence obtained by separating the recovery phase between ELMs from the instantaneous ELM burst phase.

This Letter presents the dependence of the energy confinement time during the inter-ELM phase τ_E^{int} on edge collisionality ν^* and poloidal Larmor radius ρ_{pol}^* at constant poloidal beta β_{pol}, i.e., $\tau_E^{int} = \tau_B f(\nu^*, \rho_{pol}^*)$ where τ_B denotes the Bohm diffusion time. To accomplish this study, a data set of ELMy H mode plasmas heated by neutral beam (NB) in a JT-60U tokamak has been used. Then, local electron heat transport between ELMs is examined from the change of ELM perturbation profiles. This study is basically motivated by the prediction of the heat transport between ELMs (which is apart from the prediction of ELM size) in the reactor operational regime characterized by sufficiently low $\nu^*(\sim 0.03)$ and small $\rho_{pol}^*(\sim 0.01)$ [9]. Hereafter, ν^*, ρ_{pol}^*, and β_{pol} represent the values evaluated at the top of ETB using the averaged poloidal field unless otherwise specified. In addition, this Letter introduces the normalized energy confinement time τ_E^* and the normalized heat diffusivity χ^*. The asterisk for τ_E and χ denotes the value normalized to τ_B and the Bohm diffusivity $\chi_B(= T_e/16eB)$, respectively.

Figure 1 shows a typical time evolution of plasma energy W in the ELMy H mode phase. During the recovery phase between ELMs, the plasma energy increases with a

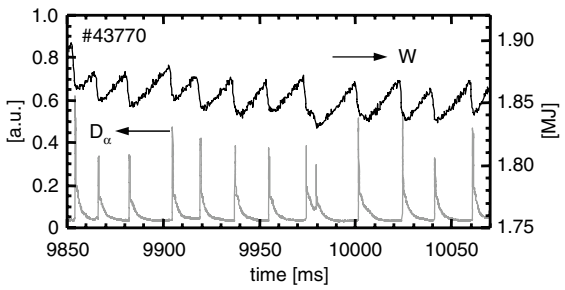

FIG. 1. A typical waveform of the ELM activities shown by D_α emission intensity and plasma energy W.

time constant τ_E^{int} determined by the energy balance for heat flux from the plasma core and transport loss crossing the separatrix described by the following equation:

$$\frac{dW}{dt} = P_{heat} - \frac{W}{\tau_E^{int}} - \Delta W_{ELM}\delta(t - t_{ELM}). \quad (1)$$

Here, P_{heat} denotes the source heating power crossing the separatrix, ΔW_{ELM} and t_{ELM} are the plasma energy released by an ELM burst and the time when ELM events occur, respectively. In Eq. (1), the second and third terms on the right hand side represent the diffusive heat fluxes of the inter-ELM transport loss and the periodic heat loss associated with the ELMs, respectively. In a steady-state phase in a time scale much longer than an ELM event, i.e., $\overline{dW/dt} = 0$ where the bar denotes the value averaged over ELM cycles, Eq. (1) becomes

$$P_{heat} \simeq P_{int} + P_{ELM} \quad (P_{ELM} = f_{ELM}\Delta W_{ELM}), \quad (2)$$

where P_{int} and P_{ELM} are the loss powers of the inter-ELM transport and ELMs, respectively, and f_{ELM} denotes the ELM frequency. In a situation of steady state, P_{heat} is assigned to two heat loss channels of the inter-ELM loss and the instantaneous ELM heat loss. In the previous studies, it has been observed that P_{ELM} remains roughly in the range of 20%–40% of P_{heat} in type-I ELMy H modes [6,10]. Shown in Fig. 2(a) is the fraction of the power assigned from the source heat flux P_{heat} to P_{ELM} and P_{int} as a function of ν^* while keeping ρ^*_{pol} and β_{pol} fixed.

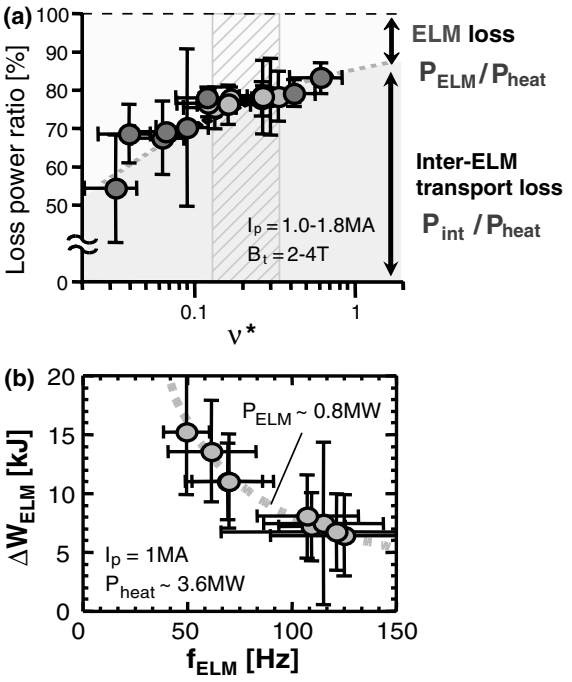

FIG. 2. (a) The fraction of the power assigned to ELM and inter-ELM transport from the power crossing the separatrix as a function of ν^*. (b) The relation between ELM frequency f_{ELM} and ELM energy loss ΔW_{ELM} at $\nu^* \sim 0.2$–0.3 and $I_p \sim 1$ MA, corresponding to the hatched area in Fig. 2(a).

The geometrical parameters are in the ranges of the ellipticity $\kappa = 1.35$–1.60, the triangularity $\delta = 0.16$–0.39, and the safety factor at 95% flux surface $q_{95} = 3.0$–4.2. In Fig. 2(a), it is obvious that the ELM loss power does not remain at a constant fraction, but the loss power ratio can be changed by ν^*. When ν^* is increased, the inter-ELM transport is enhanced and the ELM heat loss is reduced, independently of plasma configuration. Figure 2(b) shows the relation between ELM frequency f_{ELM} and ELM energy loss ΔW_{ELM} at $\nu^* \sim 0.2$–0.3 [corresponding to the hatched area in Fig. 2(a)]. The variation of f_{ELM} is given by changing the gas puffing rate. Then, ΔW_{ELM} varies inversely proportional to f_{ELM} so that P_{ELM} remains constant at fixed P_{heat}. In addition, this result indicates that the diffusive heat flux between ELMs is also kept constant at a given ν^* in spite of the wide variation of f_{ELM} and ΔW_{ELM}, e.g., $P_{int}/P_{heat} \sim 75$–80% at $\nu^* \sim 0.2$–0.3.

After the energy release associated with an ELM burst, the plasma energy starts to increase with the source heat flux due to the NB injection. To maintain a steady state in a global time scale ($\overline{dW/dt} = 0$), the plasma energy is recovered with a time constant τ_E^{int} to the level just before ELM burst occurs. Therefore, the size of the ELM energy drop ΔW_{ELM} controlled by the edge MHD instability and energy confinement time τ_E^{int} involved in the recovery of the edge plasma to its pre-ELM state following the ELM collapse, determine, consequently, the time interval between ELMs or f_{ELM}.

In order to understand the process responsible for heat transport during the inter-ELM phase, we examine the dependence of τ_E^{int} on the edge nondimensional parameters since the recovering heat flux is localized particularly in the peripheral region affected by ELM crash. We will first discuss the ν^* dependence. Figure 3(a) shows the dependence of the normalized energy confinement time between ELMs $\tau_E^{int*}(\equiv \tau_E^{int}/\tau_B)$ on ν^* and ρ^*_{pol}. For the ν^* dependence, the variation of ν^* is selected with keeping constant $\rho^*_{pol} \simeq 0.05$, $\beta_{pol} \simeq 0.3$, $q_{95} \simeq 4.0$, and $\delta \simeq 0.35$. This is done by varying the plasma current I_p with adjusting the edge plasma density. It is obviously seen that the energy confinement between ELMs is significantly improved as ν^* is reduced, satisfying the relation of $\tau_E^{int*} \propto \nu^{*-0.6}$. The energy confinement time in a global time scale $\bar{\tau}_E^*$ shows weaker collisionality dependence given as $\bar{\tau}_E^* \propto \langle \nu^* \rangle^{-0.35}$, where the bracket $\langle \cdot \rangle$ denotes the volume-averaged value over the whole plasma. This dependence of $\bar{\tau}_E^*$ is almost consistent with that previously studied in the nondimensional transport analysis in JT-60U [11]. Figure 3(a) is indicative of a more collision-based heat transport during the inter-ELM phase.

Next, we will discuss the ρ^*_{pol} dependence. It is basically hard to keep a sufficient range of ρ^*_{pol} at constant ν^* and β_{pol} in ELMy H mode plasmas. This is because of the existing edge stability boundary for ELMs. In practice, the edge pressure scales empirically as $nT \propto I_p^{1.4-1.6}$ [12]. Then, one can find it difficult to conduct the pure

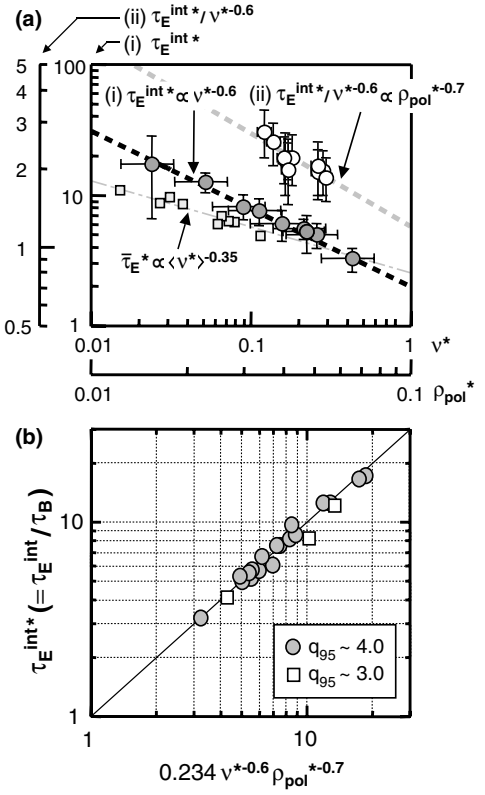

FIG. 3. (a) The dependence of $\tau_E^{int*}(=\tau_E^{int}/\tau_B)$ on (i) ν^* (shaded circle; $\rho_{pol}^* \simeq 0.05$ and $\beta_{pol} \simeq 0.3$) and (ii) ρ_{pol}^* (open circle; $\beta_{pol} \simeq 0.25$). Shaded square indicates the dependence of $\bar{\tau}_E^*$ on $\langle\nu^*\rangle$. (b) Comparison of τ_E^{int*} with the scaling expression based on ν^* and ρ_{pol}^* at $q_{95} \simeq 4.0$ and $\delta \simeq 0.3$ (shaded circles). Lower q_{95} case is also shown as open square.

$\rho_{pol}^*(\propto \sqrt{T}/I_p)$ scan at fixed $\nu^*(\propto n/T^2)$ due to the strong colinearity with $\beta_{pol}(\propto nT/I_p^2)$. Instead of the pure ρ_{pol}^* scan, the knowledge of the ν^* dependence can be used to infer the ρ_{pol}^* dependence from the data set in which ν^* and ρ_{pol}^* vary together while keeping β_{pol} fixed. In Fig. 3(a), the variation of τ_E^{int*} normalized to $\nu^{*-0.6}$ as a function of ρ_{pol}^* is shown. The variation of ρ_{pol}^* is selected at fixed $\beta_{pol} \simeq 0.25$, $q_{95} \simeq 4.0$, and $\delta \simeq 0.35$ while ν^* varies in the range of 0.08–0.36. Then, it appears that τ_E^{int*} becomes larger at smaller ρ_{pol}, satisfying $\tau_E^{int*} \propto \rho_{pol}^{*-0.7}$. Shown in Fig. 3(b) is the distribution of τ_E^{int*} expressed by ν^* and ρ_{pol}^* for the cases of $q_{95} \simeq 4.0$ and $\delta = 0.30$–0.35. Employing the regression based on the power law (log-linear) expression, the best fit is obtained at $\tau_E^{int*} \propto \nu^{*-0.6}\rho_{pol}^{*-0.7}$. It may be worth pointing out in passing that the rms error for the functional form of $\tau_E^{int*} = f(\nu^*, \rho_{pol}^*)$ is 0.55, which is reduced by ~40% from the case where τ_E^{int*} is evaluated as a function of only ν^* (RMSE = 0.90). In order to consider the effect of magnetic structure on the inter-ELM heat transport, Fig. 3(b) also plots τ_E^{int*} for the case of lower q_{95}. It is seen that τ_E^{int*} at lower $q_{95}(\simeq 3.0)$ follows closely the expression for the higher $q_{95}(\simeq 4.0)$, suggesting no strong dependence of q_{95} on the inter-ELM heat transport.

We now focus on the local heat diffusivity during the inter-ELM phase. Figure 4 plots the relative perturbations of the electron temperature profiles due to an ELM for two cases of (A) low $\nu^*(= 0.02)$ and (B) high $\nu^*(= 0.22)$ at fixed $\rho_{pol}^*(\simeq 0.05)$ and $\beta_{pol}(\simeq 0.3)$. While profiles of $\Delta T_e/T_e$ become larger near the plasma boundary for both cases, the amplitude of the relative perturbation is relatively large for the low ν^* case. Besides, the energy drop at low ν^* involves the relative perturbation of the T_e profile across an ELM that extends radially more inward. Indeed, the measured energy pulse expelled by ELM bursts $\Delta W_{ELM}/W$ in the low ν^* case is larger by a factor of 1.8 than that in the high ν^* case. During the inter-ELM phase, the energy equivalent to ΔW_{ELM} is replenished by the heat flux from the plasma core during the time interval between ELMs Δt^{int}. To evaluate the time derivative of electron energy, the changes of the n_e and T_e profiles between ELMs are evaluated with the fast ECE radiometer and Thomson scattering measurements with a YAG laser system. As seen in Fig. 1, an ELM burst occurs in many cases much earlier than the plasma energy W reaches the steady-state level. Then, the electron heat diffusivity averaged during the inter-ELM phase is derived from the electron conductive heat flow given as

$$Q_e^{cond} - \frac{1}{r}\int_0^r \frac{3}{2}\frac{\Delta(n_e T_e)_{ELM}}{\Delta t_{int}} r dr = n_e \chi_e^{int}\frac{dT_e}{dr}, \quad (3)$$

where Q_e^{cond} denotes the electron conductive power density, $\Delta(n_e T_e)_{ELM}$ is the change of the electron pressure across an ELM, and χ_e^{int} is the electron heat diffusivity during the inter-ELM phase. Since the change of the number of electrons between ELMs $(dN_e/dt)^{int}$ is negligibly small compared to the source electron particle flux, the electron convective power density during the inter-ELM phase hardly differs from that evaluated in a global time scale. The radiation loss power is ~20% of the source

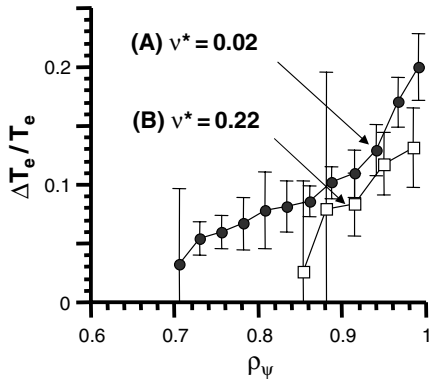

FIG. 4. Relative perturbations to the electron temperature profiles due to an ELM for the cases of (A) low $\nu^*(= 0.02)$ and (B) high $\nu^*(= 0.22)$. The measurement locations are converted to normalized poloidal magnetic flux radius ρ_ψ

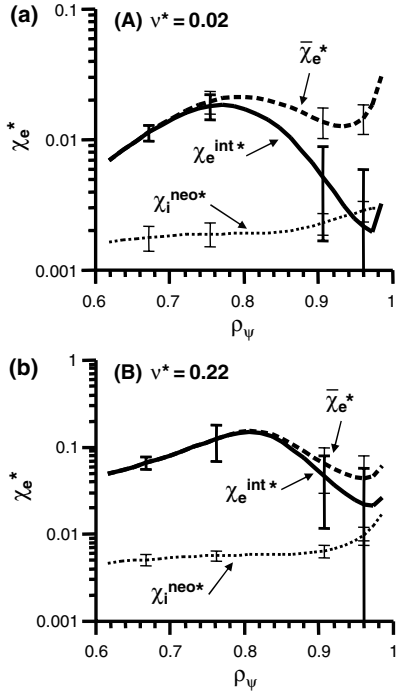

FIG. 5. Profiles of the electron heat diffusivity during the inter-ELM phase χ_e^{int*} for the cases of (a) low $\nu^*(= 0.02)$ and (b) high $\nu^*(= 0.22)$. The electron heat diffusivity in a global time scale $\bar{\chi}_e^*$ and the ion neoclassical heat diffusivity χ_i^{neo*} [13] are also shown for reference.

heating power for both cases. Figure 5 shows the profiles of the normalized electron heat diffusivity during the inter-ELM phase $\chi_e^{int*}(= \chi_e^{int}/\chi_B)$ for the cases shown in Fig. 4. In comparison with the electron heat diffusivity evaluated in a global time scale $\bar{\chi}_e^*$, it is seen in both cases that the reduction of χ_e^{int*} is localized in the plasma edge region affected by ELM perturbation. In particular, χ_e^{int*} around the position of the ETB ($\rho_\psi \geq 0.95$) is significantly reduced to the level of ion neoclassical heat diffusivity χ_i^{neo*}. In the banana regime ($\nu^* < 1$), the normalized neoclassical heat diffusivity χ^{neo*} scales as $\nu^* \rho_{pol}^* q^0$ at a given inverse aspect ratio ϵ in the poloidal system. Figure 5 amounts to saying that the ν^* dependence of χ_e^{int*} is similar to that of the neoclassical heat transport in the peripheral region. In practice, the reduction in χ_e^{int*} is not seen in the plasma core region. In that respect, we can presume that the increased energy confinement time between ELMs at low ν^* is mainly attributed to the reduction of heat diffusivity in the plasma edge region where the pressure profile affected by an ELM burst recovers to its pre-ELM state. In addition, χ^{neo*} does not depend explicitly on the safety factor. As regards the edge heat diffusivity, this is not in conflict with no q_{95} dependence of τ_E^{int*} shown in Fig. 3(b). However, it is noted that χ_e^{int*} at the plasma edge is not reduced to the level of electron neoclassical heat diffusivity $\chi_e^{neo*}(\sim\sqrt{m_e/m_i}\chi_i^{neo*})$. Since the time scale of electron-ion heat exchange becomes shorter than τ_E^{int} at higher ν^*, the relation between the electron-ion energy relaxation process and the inter-ELM heat transport should be quantified in a next study.

In summary, the reduction of electron heat diffusivity between ELMs to the level of ion neoclassical transport was found in the plasma edge region affected by an ELM burst. As ν^* becomes smaller, the heat flux assigned to the heat transport between ELMs is reduced and the ELM loss power is enhanced. The energy confinement time during the inter-ELM phase τ_E^{int*} increased at low ν^* and small ρ_{pol}^*, satisfying $\tau_E^{int*} \propto \nu^{*-0.6}\rho_{pol}^{*-0.7}$. From the result presented in this Letter, it is expected that the heat transport between ELMs is sufficiently reduced at the plasma edge in the reactor operational regime. However, one can also expect that it is not simple to achieve the high energy confinement simultaneously with small ELM losses particularly at low ν^*. In fact, it is observed that ΔW_{ELM} in the type-I ELMs can be larger with decreasing ν^* [6–8], while the ρ_{pol}^* dependence of ΔW_{ELM} has not systematically been investigated in detail because the ρ_{pol}^* value in the reactor is much smaller than accessible in the present large tokamaks. As shown in Fig. 2(a), the reduced heat transport is always accompanied by a large ELM loss power at low ν^*. It is observed that the plasma geometrical configuration influences largely not only on the amplitude and frequency of ELM perturbations, but also on the energy confinement properties. Therefore, characterization of the inter-ELM heat transport as well as the instantaneous ELM loss in a variety of geometrical parameters in the low ν^* regime is required for realizing high integrated performance in future devices.

The authors are grateful to Dr. H. Ninomiya, Dr. M. Kikuchi, and Dr. M. Nagami for their encouragement and helpful advice. The diligent support of the JT-60U team is also cordially acknowledged.

[1] F. Wagner *et al.*, Phys. Rev. Lett. **49**, 1408 (1982).
[2] H. Zohm, Plasma Phys. Controlled Fusion **38**, 105 (1996).
[3] P. B. Snyder *et al.*, Phys. Plasmas **9**, 2037 (2002).
[4] P. B. Snyder *et al.*, Plasma Phys. Control. Fusion **45**, 1671 (2003).
[5] A. Leonard *et al.*, Plasma Phys. Control. Fusion **44**, 945 (2002).
[6] A. Loarte *et al.*, Plasma Phys. Control. Fusion **44**, 1815 (2002).
[7] H. Urano *et al.*, Plasma Phys. Control. Fusion **45**, 1571 (2003).
[8] N. Oyama *et al.*, Nucl. Fusion **44**, 582 (2004).
[9] M. Shimada *et al.*, Nucl. Fusion **44**, 350 (2004).
[10] W. Suttrop *et al.*, Plasma Phys. Control. Fusion **40**, 771 (1998).
[11] H. Shirai *et al.*, Plasma Phys. Control. Fusion **42**, 1193 (2000).
[12] J. G. Cordey *et al.*, Nucl. Fusion **43**, 670 (2003).
[13] S. P. Hirshman *et al.*, Nucl. Fusion **21**, 1079 (1981).